Thermophysical Properties of Foliated Graphite/Nickel Reinforced Polyvinyl Chloride Nanocomposites

A. A. Al-Ghamdi,[1] Falleh Al-Salamy,[2] Omar A. Al-Hartomy,[1,3] Attieh A. Al-Ghamdi,[4] A. M. Abdel Daiem,[1,5] Farid El-Tantawy[6]

[1]*Faculty of Science, Department of Physics, King Abdulaziz University, Jeddah, Jeddah 21569, Kingdom of Saudi Arabia*
[2]*Faculty of Science, Department of Mathematics, University of Tabuk, Tabuk, Kingdom of Saudi Arabia*
[3]*Faculty of Science, Department of Physics, University of Tabuk, Tabuk, Kingdom of Saudi Arabia*
[4]*King Abdulaziz City for Science and Technology, Electronics, Communications, and Photonics Program, Riyadh, Kingdom of Saudi Arabia*
[5]*Faculty of Science, Department of Physics, Zagazig University, Zagazig, Egypt*
[6]*Faculty of Science, Department of Physics, Suez Canal University, Ismailia, Egypt*

Received 20 April 2011; accepted 6 June 2011
DOI 10.1002/app.35062
Published online 12 October 2011 in Wiley Online Library (wileyonlinelibrary.com).

ABSTRACT: A novel, polymer-based foliated graphite/nickel nanocomposites with high thermal conductivity, mechanical properties, and low dielectric constant was developed. The network structure of polyvinyl chloride (PVC) reinforced foliate graphite and nickel nanoparticles (GN) were tested in terms of X-ray diffraction (XRD), scanning electron microscope (SEM), energy dispersive x-ray analysis (EDX), and thermal-gravimetric analyses (TGA). Thermogravimetric analysis revealed a large improvement in the thermal stability of PVC/GN nanocomposites. Thermal conductivity and diffusivity of the composites increased with increasing GN content and temperature. The obtained experimental thermal conductivity result are compared with the existing theoretical models. The measured values of thermal conductivity were in excellent agreement with those calculated from the Agari model. In addition, specific heat, coefficient of thermal expansion (TEC), micro porosity, and crosslinking density (CLD) of composites were investigated. The mechanical properties such as tensile strength, tensile modulus, hardness, and elongation at break of the nanocomposites were improved with inclusion GN which is proportional to GN content. Finally, the dielectric properties of PVC/GN nanocomposites as a function of frequency have been investigated in details. © 2011 Wiley Periodicals, Inc. J Appl Polym Sci 124: 1144–1153, 2012

Key words: polyvinyl chloride; graphite–nickel nanoparticles; nanocomposites; network structure; thermal properties

INTRODUCTION

The development of conducting polymer nanocomposites (CPCs) containing nanosized filler has recently become a popular topic in material science due to their large potential applications in various fields such as, microprocessors and memory chips, bipolar plates for use in fuel cells, biosensor, and others.[1–5] One approach for improving the thermal properties of a polymer is via the inclusion of a conductive filler materials, such as carbon black, metal, ceramic, etc.[6–10] Among the conducting fillers, carbon-based materials such as graphite has attracted a great attention due to its chemical stability under ambient conditions, high electrical conductivity, a rather low cost and simple synthesis, light weight, large surface area/volume ratio, associated with a large contact area among the filler and the polymer matrix, high thermal conductivity, a unique layered nanostructure, less material requirement for percolation, and ease of processing into host polymers.[11–20] CPCs are also attractive for electronic packaging, heat exchangers, appliances, machinery, integrated circuits and other applications requiring high thermal conductivity to dissipate the huge heat and low dielectric constant to avoid signal propagation delay.[21–25] With increasing power of micro or nano electronics, thermal management such as heat release from electronic chips is a fatal problem for the electronic industry that limits the performance, speed, life time, reliability, quality of electronic devices.[26–30] Thus, knowing thermophysical properties of the conducting nanocomposite materials has gained significant importance in the design of new systems and quantifying the role of composites in the application. In fact, the temperature fields in composite materials cannot be determined unless the thermal properties of the media are known.[31,32] However,

Correspondence to: F. El-Tantawy (faridtantawy@yahoo.com).

the fatal shortcoming for polyvinyl chloride (PVC) in such applications is its poor thermal conductivity only 0.014 W/m/K, which is why PVC is usually and traditionally used as excellent electrical insulating material.[33,34] If a PVC based material with enhanced thermal conductivity could be developed, combined with its fairly good processability, low dielectric constant and mechanical properties, it will become an excellent substitute for metals and ceramics in heat transfer and heat sinks in electronic packaging applications, thermal assemblies of the fire box as well as brake discs for airplane in the aeronautical, astronautical, tunnel oven conveyor belts (in particular for the food industry), architectural coverings, and civil fields.[35,36] The advantages of thermally conductive polymer compared to typically used metals and ceramics include improved corrosion resistance, lighter weight, and the ability to tailor the conductivity to any desirable utilization technology. To the best of our knowledge, no information is available on detailed studies of the thermal and dielectric properties of PVC/GN nanocomposites. The objective of this contribution is to investigate the effects of GN content on the network structure of composites. To this end, the thermal, mechanical, and dielectric properties of composites were investigated in details and the experimental results of thermal conductivity were compared with theoretical models.

EXPERIMENTAL PART

Material description

Natural flake graphite, purchased from Shandong Qingdao Graphite Company (Qingdao, China), with an average diameter of 500 μm is used for preparing the expanded (exfoliated) graphite. Commercial concentrated sulfuric acid and nitric acid from Egyptian Chemical Company (Cairo, Egypt) was used as chemical intercalant and oxidizer to prepare exfoliated graphite. Alcohol (95% v/v) and distilled water were used as solvent for the preparation of foliated (nanosheets) graphite. PVC was obtained from Tokyo Chemical Industry (Tokyo, Japan). Nickel powder was supplied by Wako Chemical Company with a particle size of 10 μm.

Preparation of exfoliated graphite

Natural flake graphite was first dried in a vacuum oven for 24 h at 100°C. A mixture of concentrated sulfuric acid and nitric acid (ratio 4 : 1, v/v) was slowly added to a glass flask containing graphite flakes with vigorous stirring. After 24 h of reaction the acid-treated graphite flake was filtered and washed with deionized water until the pH level of the solution reached 6.4. After being dried at 100°C for 24 h, the resulting graphite intercalation compound was subjected to a thermal shock at 1100°C for 50 s in a muffle furnace to form exfoliated (Expanded) graphite).

Preparation of foliated graphite nanosheets

We sonicated the expanded graphite in alcohol solution to gain shiny graphite powder. In a typical synthetic procedure for foliated graphite nanosheets, 1 g of exfoliated graphite was mixed and saturated with 400 mL alcohol solution consisting of alcohol and distilled water with a ratio of 70 : 30 for 24 h. Then the mixture was subjected to ultrasonic irradiation with a power 400 W for 24 h. After 24 h of sonication, exfoliated graphite particles were effectively fragmented into foliated (nanosheets) graphite. The foliated graphite dispersion was then filtered and dried at 100°C to remove residual solvents. The as-prepared foliated graphite powder is referred as graphite nanosheets.

Preparation of nickel nanoparticles

The starting material for ball milling was Ni (250 mesh) with purity above 99.9%. The Ni powder was placed in a stainless steel vial with stainless steel balls of 10 mm diameter each. Ball-to-powder ratio of 15 : 1 was mixed in a planetary miller (Marconi MA 350 ball miller) at 400 rpm under argon atmosphere for 10 h.

Preparation of PVC/GN nanoconducting composites

The conducting fillers utilized here are composed of graphite nanosheets, with mean diameter of roughly 20 mm and average thickness of about 13 nm (the number of sheets in the platelets is 100), and Ni with an average particles size of 30 nm. Mixtures of as-prepared graphite nanosheets with conducting nickel nanoparticles 90/10 wt % were grinded together in a grinding machine for 1 h. The as received conducting mixtures were then added to the PVC matrix and mixed by grinding machine for 30 min. The whole mixtures were transferred to a hot press at 40 KN/m^2 under temperature of 185°C for 10 min. Several batches of PVC/GN weight ratios were considered: 95 : 05, 90 : 10, 85 : 15, and 80 : 20, respectively, and abbreviated as GN5, GN10, GN15, and GN20, respectively.

Instruments and methods

Crystal structures of as synthesized graphite, nickel, and graphite–nickel compound powders were

investigated by X-ray diffraction (XRD, D/Max 2200V, Rigaku, Japan) with Cu $k\alpha$ ($\lambda = 1.5406$ A°) radiation. The average crystallite sizes (D) were calculated from X-ray peak broadening by Debye–Scherrer equation using the full width at half maximum (FWHM) data.

The Debye–Scherrer equation is[10]:

$$D = F\,\lambda/\beta\cos\theta \tag{1}$$

where λ is the wavelength of the X-ray radiation, F is a constant generally taken to be 0.9, θ is the diffraction angle, and β is the full width at half maximum given by:

$$\beta^2 = \beta_0^2 - \beta_i^2$$

where β_0 and β_i are the width from the observed X-ray peak and the width due to instrumental effects, respectively.

The morphology of composites was analyzed by using a scanning electron microscopy (SEM, JSM-5310 LVB, JEOL). The specimens were coated with gold to avoid charging using a vacuum evaporator (JEOL, GEE 500) and the voltage used was 15 kV.

Energy dispersive X-ray spectrometer (EDS, Horiba EMAX) was used to semi-quantitatively analyze the chemical composition of the synthesized powders. EX-350 software was used to analyze the obtained results.

Thermogravimetric analysis (TGA) was carried out on a Shimadzu TGA-50H thermogravimeter analyzer and the sample was heated from room temperature to 800°C at a rate of 10°C/min in a steady flow of nitrogen.

Thermal conductivity and specific heat was measured using thermal in flash technique (Tokyo, Japan) for non steady state measurement of thermal properties.[1] The measurements were performed with bulk samples ($20 \times 20 \times 6$ mm^3) by putting the sensor (2 mm diameter) between two slabs of material. The sensor supplied a heat pulse of 0.05 W for 30 s to the sample and the associated change in temperature was recorded. Testing temperature ranged from room temperature 20°C to 150°C.

The thermal expansion coefficient (TEC) for composites was detected by thermal dilatometry (Netzsch Geratebau E 404).

In mechanical properties, dumbbell-shaped specimens were cut from the molded perform sheets for the measurement of tensile properties. Tensile strength (TS), tensile modulus (TM), and elongation at break (EB) were obtained from engineering stress–strain diagrams using an Instron 3366 universal testing machine (Instron Corporation, Norwood, MA) with adequate ventilation was employed to conduct tensile tests at room temperature according to the procedure described in ASTM D412. A total of at least five specimens were analyzed for each composite. Data were logged to a desktop computer at a frequency of 50 Hz. Hardness (H) shore D of the specimens is performed as per ASTM D 2240, using a LECO LM 100 hardness tester (Leco Corporation, St. Joseph, MI) at room temperature.

To measure the dielectric properties two terminal silver electrodes of diameter 20 mm was used to ensure the contact resistance. Capacitance and dissipation factor of PVC/GN nanocomposites were measured at constant 2 V AC using an RCL bridge (3531ZHitester, Hioki, Japan) and the overall frequency range was 1–18 GHz.

Using the equilibrium degrees of swelling (tetrahydrofuran a solvent for PVC), it is possible to calculate the crosslinking density (CLD) and is given by the following equation[37]:

$$\mathrm{CLD} = \frac{\rho_c N_A}{M_a} \tag{2}$$

where ρ_c is the composite density, N_A is the Avogadro number, and M_a is the average molar mass between crosslink's and is given by the following equation:

$$M_a = -\frac{(V_m\rho_c)\left(V_s^{\frac{1}{3}} - \frac{V_s}{2}\right)}{\ln(1-V_s) + V_s + \chi V_s^2} \tag{3}$$

where V_m is the molar volume (mL/mol), V_s is the volume fraction of polymer in the swollen gel and is given by[38]:

$$V_s = \frac{(\omega_1/\rho_c)}{(\omega_1/\rho_c) + (\omega_2/\rho_s)} \tag{4}$$

where ω_1 and ω_2 are the weights of dry sample and solvent, respectively, and ρ_s is the density of the solvent, and χ is the Flory–Huggins interaction parameter between solvent and polymer, and is given by the following formula[39]:

$$\chi = 0.432 - 0.321 - 0.036\ V_s^2 \tag{5}$$

Microporosity (P) of PVC/GN nanocomposites is calculated from the relation[2,3]:

$$P = 1 - V_f\left(\frac{\rho_c - V_f\rho_f}{\rho_p}\right) \tag{6}$$

where ρ_f and ρ_p are the densities of filler and polymer matrix, respectively. The densities are measured according to the Archimedes' method at room temperature. V_f is the volume fraction of filler in the composite.

RESULTS AND DISCUSSION

Microstructure observations

Phase composition and phase purity of the as-prepared samples were identified by X-ray patterns. X-ray pattern of (a) foliated graphite nanosheets, (b) nickel nanoparticles, and (c) graphite–nickel compound is depicted in Figure 1. In Figure 1(a), a strong and wide crystalline graphite peak at 2θ of 26.5° and weak peak at 2θ of 54.8° were observed in the x-ray powder diffraction pattern, resulting from the diffraction of (1 1 1) and (2 2 2) planes of the graphite, respectively. The crystal structure is retained and the interplaner spacing in *c*-axis is kept at 3.35 Å. The diffraction peaks of graphite match well with the inverse cubic spinel structure (JCPDS 19-0629). The average crystallite size *D*, calculated using the Debye–Scherer equation, was roughly about 13 nm based on the main peak (1 1 1). Figure 1(b) shows the X-ray patterns of as-prepared Ni nanoparticles with average size 30 nm. Two characteristic peaks for nickel 2θ = 44.5° and 2θ = 51.8° corresponding to Miller indices (1 1 1) and (2 0 0) were observed. The appearance of those peaks reveal that the resultant particles form pure face centered cubic (fcc) nickel for these samples (JCPDS, No. 04-0850). In Figure 1(c), the XRD pattern of graphite–nickel (GN) compound revealed the characteristic peaks of both the graphite and nickel. Peaks were observed at 2θ = 26.5°, 2θ = 44.5°, and 2θ = 51.8°, which is in agreement with the XRD peak of the crystalline GN compound.[1]

To assess the surface chemical composition of as-prepared GN sample we have used the energy dispersed X-ray spectroscopy (EDX), which is attached to the SEM. Figure 1(d) is showing the EDX spectrum of GN sample (Indices of the peaks are specified above the peaks). Observation of the EDX spectrum reveals that the signatures of graphite and nickel are 80 : 20 wt %, indicating that our GN sample is purely consisting of graphite and nickel elements with the desired proportion. The result clearly indicates that nickel and graphite are intercalated together as supported by XRD spectra.

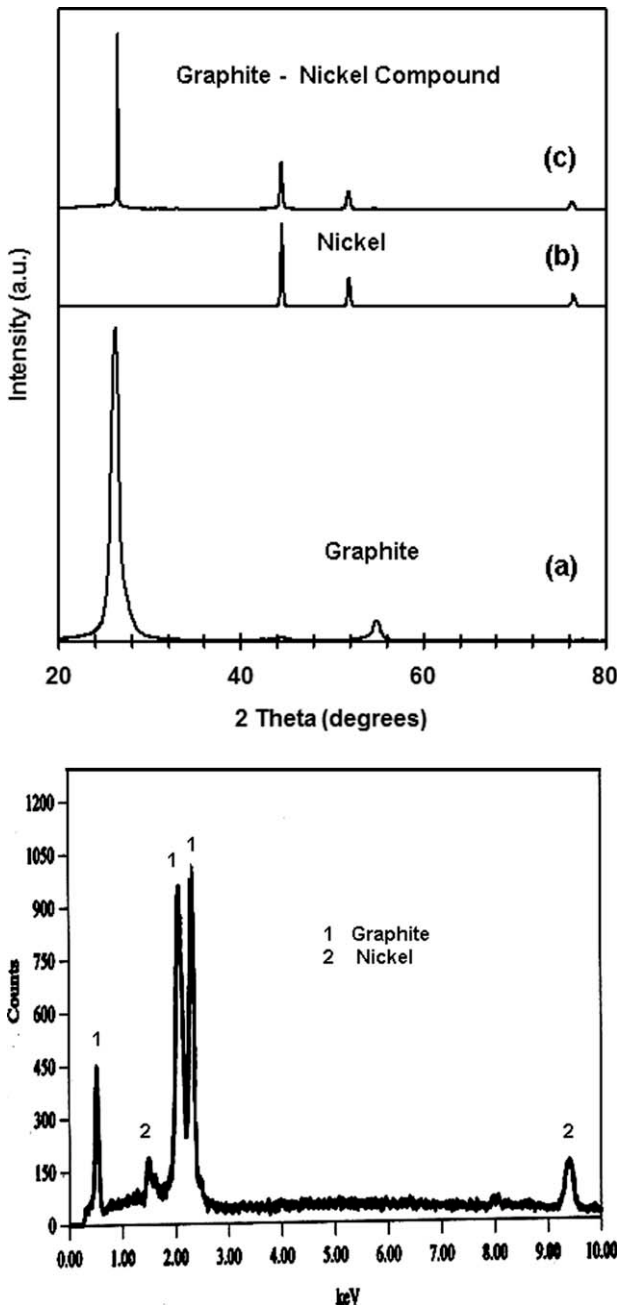

Figure 1 XRD diffraction of (a) foliated Graphite, (b) Ni compound, (c) GN compound, and (d) EDX spectra of GN20 sample.

Before any composite morphology observation, it is necessary to characterize with enough precision the filler particle morphology and filler distribution into matrix. The typical scanning micrographs (SEM) of as-prepared foliated graphite nanosheets is depicted in Figure 2(a). We can clearly observe that the ultrasonic radiation breaks down the worm-like structure and reduces its size, resulting in individual graphite nanoplatelets. It revealed that the exfoliated graphite was tore to platelets with an average diameter of 10 μm. The as-prepared foliated graphite nanoplatelets possessed a high aspect ration (width-to-thickness) of around 600 and with apparent density of about 0.018 g/cm^3 (measured by Archimedes technique), much smaller than that of the original flake graphite, 2.26 g/cm^3.[2–5]

The typical SEM image of GN20 sample is depicted in Figure 2(b). In Figure 2(b), it is clear that PVC chain is effectively incorporated into the galleries of foliated graphite layers. Such good dispersion of the GN nanoparticles into the PVC matrix may contribute to enhancing the thermal properties and skeleton molecular structure of nanocomposites. It is suggested that the well dispersion of GN in

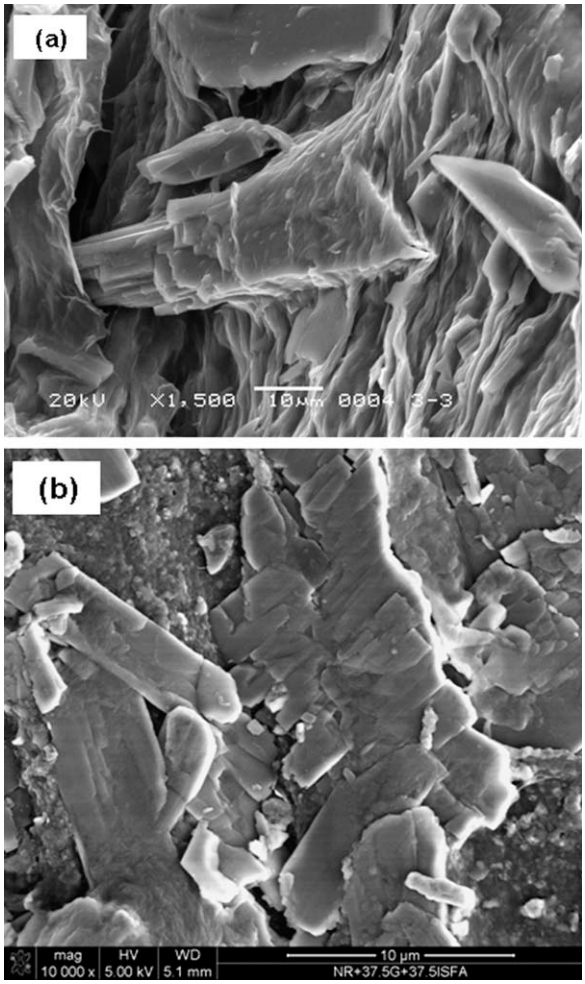

Figure 2 Scanning electron microphotographs of (a) exfoliated graphite and (b) GN20 sample.

PVC matrix could enhance the surface-to-volume ratio of GN and interfacial factors, which could on the whole contribute to potent thermophysical properties effect for the nanocomposites. Furthermore, we can clearly observe that the GN nanoparticles were distributed quite uniformly within the PVC matrix and no aggregates can be seen in the composite. Because of this especial structure, the interfacial affinity of GN nanoparticles with the PVC matrix increased and led to ensured thermal stability entire nanocomposites.

Thermogravimetric analysis

The thermal stability of composites was determined using a thermogravimetric (TGA) analyzer. The thermal stability of foliated graphite, green PVC, and PVC/GN nanocomposites are depicted in Figure 3. It is seen that there is no any weight loss for graphite nanosheets up to 770°C, thereafter there is a weight loss of about 1.5 weight percent. On the other hand, the TGA curves reveal that there are three main degradation stages. The first weight loss occurs at 180°C, which correspond to the removal of water. The second stage is between 300°C and 450°C, which is responsible for the scission of the PVC main chains; whereas the third stage occurs between 500 and 700°C, during which the C—C and C—O bonds on the main chain are further destroyed due to the oxidation.[15,16] The temperature of 5% weight loss was 235, 247, 260, 273, and 300°C, respectively, for the samples green PVC, GN5, GN10, GN15, and GN20, respectively. This indicates the positive effect of GN nanoparticles on the thermal stability of the nanocomposites. It is worthily to mention that the increase in decomposition temperature was attributed to the enhancement of interaction between the PVC matrix and the GN nanoparticles, which limited the segmental movement of the PVC.[1,2] Furthermore, the enhances stability of nanocomposites can be attributed to the homogeneous distribution of GN particles as well as the tortuous path in the composites that hinders diffusion of the volatile decomposition products in the composites compared to that in green PVC.[21–24]

Thermal conductivity of GN reinforced nanocomposites

Understanding of thermal properties of the conducting polymer nanocomposites leads to important applications in electronic packaging and other engineering disciplines. The thermal properties like thermal conductivity, thermal diffusivity, and specific heat of composites is a function of volume fraction of filler, size, shape and aspect ratio of filler, phase distribution, thermal conductivity values of the individual components, degree of interfacial thermal

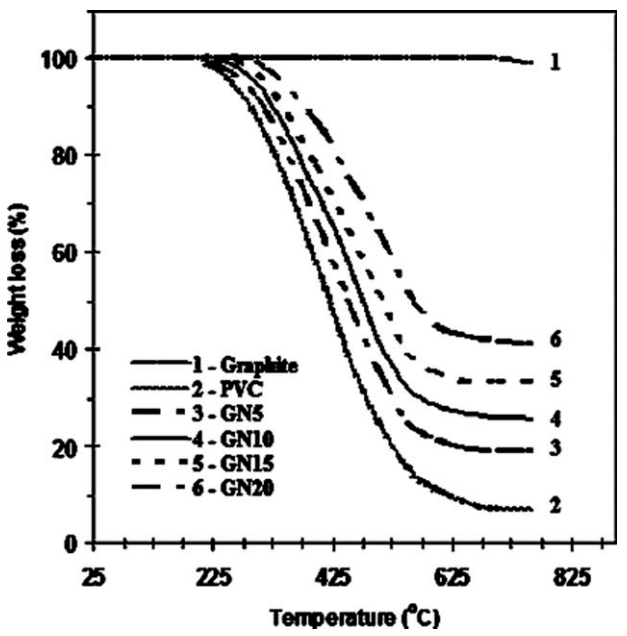

Figure 3 The thermo-gravimetric (TGA) of foliated graphite, green PVC, and PVC/GN nanocomposites.

contact between components etc.[16,17] The variation in the experimental thermal conductivity (k) of PVC/GN nanocomposites as a function of GN content is depicted in Figure 4. It is clear that a nonlinear increase in the thermal conductivity was observed with an increase in the content of GN into nanocomposites. It should be pointed out that the thermal conductivity of PVC/GN nanocomposites is higher than that of green PVC. This behavior can be explained on the basis of CLD of composites and interfaces existing between GN nanoparticles and PVC matrix in the entire the composites. When GN nanoparticles are reinforced into green PVC, they reduce the free volume and increase the number of elastically effective chains resulting in increase of the cross linking density of composite.[1] This improves the thermal conduction in whole composites over the green PVC polymer matrix.

However, numerous theoretical models were used to predicting the thermal conductivity of composites as a function of filler volume fraction. The following models are used to compute the thermal conductivity of PVC/GN nanocomposites:

1. Maxwell–Eucken Model (MEM)[10,11]:

$$k_c = \frac{k_p\left[2k_p + k_f + 2V_f\left(k_f - k_p\right)\right]}{2k_p + k_f - V_f\left(k_f - k_p\right)} \tag{7}$$

2. Bruggeman Model (BM)[16]:

$$1 - V_f = \frac{\left(k_f - k_c\right)\left(k_p/k_c\right)^{1/3}}{k_f - k_p} \tag{8}$$

3. Geometric Mean Model (GMM)[29]:

$$k_c = k_f^{V_f}\, k_p^{1-V_f} \tag{9}$$

4. Effective Medium Theory Model (EMTM)[21]:

$$V_f \frac{k_f - k_c}{k_f + 2k_c} + V_p \frac{k_p - k_c}{k_p + 2k_c} = 0 \tag{10}$$

5. Cheng–Vachon Model (CVM)[29]:

$$\frac{1}{k_c} = \frac{1}{\sqrt{C\left(k_p - k_f\right)\left[k_p + B\left(k_f - k_p\right)\right]}} \times \ln \frac{\sqrt{\left(k_p + B\left(k_f - k_p\right)\right)} + \frac{B}{2}\sqrt{C\left(k_f - k_p\right)}}{\sqrt{\left[k_p + B\left(k_f - k_p\right)\right]} - \frac{B}{2}\sqrt{C\left(k_p - k_f\right)}} + \frac{1 - B}{k_p} \tag{11}$$

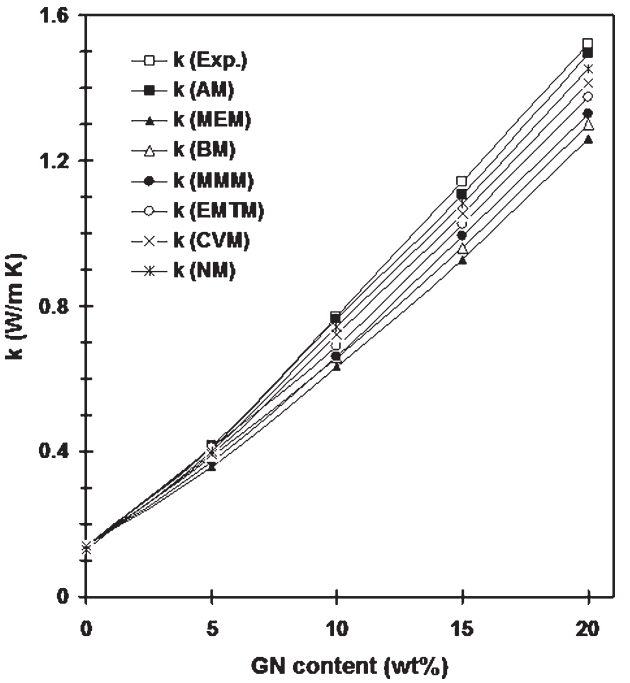

Figure 4 Measured and calculated thermal conductivity (k) versus GN content of PVC/GN nanocomposites.

where $B = \sqrt{3V_f/2}$ and $C = -4\sqrt{2/3V_f}$

6. Nielsen Model (NM)

$$k_c = \left(\frac{1 + 2\alpha\chi V_f}{1 - \chi\phi V_f}\right)k_p \tag{12}$$

where $\alpha = \frac{h}{d}$, $\chi = \frac{(k_f/k_p - 1)}{(k_f/k_p + 2\alpha)}$, and $\varphi = 1 + \left(\frac{1 - V_{\max}}{V_{\max}^2}\right)V_f$

7. Agari Model (AM)[13]:

$$\log k_c = V_f C_2 \log k_f + \left(1 - V_f\right)\ \log\left(k_p C_1\right) \tag{13}$$

where k_c, k_p, and k_f are the thermal conductivities of composites, PVC polymer matrix, and filler, respectively, V_f is the volume fraction of filler in the PVC/GN nanocomposite, h is the thickness of filler, d is the diameter of filler, $V_{\max}$ is the maximum packing factor of filler, C_1 a factor related to the structure of polymer such as crystallinity of matrix, and C_2 is a factor related to the measure of ease for the formation of conductive networks of filler.

By fitting the experimental data of the thermal conductivity of the PVC/GN nanocomposites into the Agari model, we can get the values of C_1 and C_2. The computed values of C_1 are 0.913, 0.946, 0.957, and 0.989 and C_2 are 0.923, 0.967, 0.978, and 0.989 for GN content respectively. It is observed that the values of C_1 and C_2 are close to unity. This confirmed that the GN nanoparticles are well dispersed

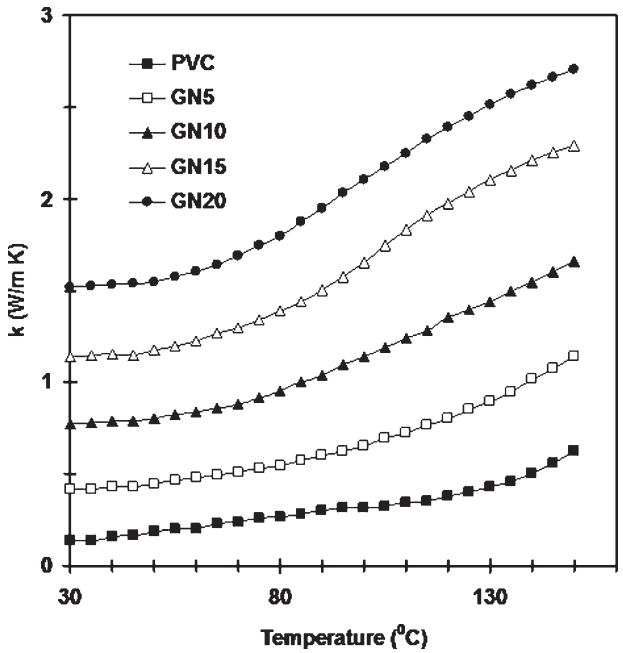

Figure 5 Thermal conductivity versus temperature of PVC/GN nanocomposites.

and form networks into PVC matrix as previously confirmed by SEM image in Figure 2(b).

The comparison of the experimental and proposed theoretical models of thermal conductivity of PVC/GN nanocomposites is shown in Figure 4. Clearly, the experimental data of the nanocomposites agreed very well with the Agari model and significantly deviates the predictions from the others proposed theoretical models. This deviation is attributed to the nanosheets shape of the filler and the special dispersion of filler entire composites.[29–36] When the effect of filler dispersion and interface interaction is not included, the predicted results are deviated from the experimental values. It is interesting to note that in Figure 4 there is a good agreement between our predictions and the measured data when the volume fraction is lower than 10 wt %. When the fiber fraction is high, the inter-fiber contacts will affect the effective thermal property. Because no thermal contact resistance[7] is considered in our model, the predicted thermal conductivities are a little lower than but still comparable with the experimental data when the volume fraction of filler is high.

The effect of GN content on the thermal diffusivity (TD), specific heat capacity (C_p) of PVC/GN nanocomposites, is depicted in Figure 5. It can clearly be seen that both TD and C_p increase with the increase of GN content into composites. This is due to that with increasing GN content into composites, the conductive phases become either very close or in direct contact with each other and the interfacial adhesion increases, leading to an increases both TD and C_p into nanocomposites. It is worth noting that when the GN fraction is high, the inter-particle contacts will affect the effective thermal property. In turn, this was another proof, besides the TGA measurements mentioned above, indicating the stability on nanocomposites enhances with increasing GN loading level. To gain further argument to the above facts we measured the *P*, CLD, and coefficient of thermal expansion (TEC) as a function of GN content as depicted in Figure 5. It is seen that both *P* and TEC decreases whereas CLD increases with increasing GN content into composites. This can be ascribed to the increase of the interfacial adhesion among filler and matrix. The decreases in the TEC of PVC/GN nanocomposites may be due to the physicochemical interaction between GN and PVC through reinforcing action. Interestingly, in Figure 5, there was a linear decreases in the *P* values with the inclusion of GN into composites. This indicates greater reinforcing nature of GN nanoparticles through confinement of PVC chains adjacent to graphite nanosheets.

The variation of thermal conductivity (*k*) and thermal diffusivity (TD) with temperature of PVC/GN is depicted in Figures 6 and 7, respectively. It is seen that there is a continuous increase of both the thermal conductivity and diffusivity with the increase of temperature of nanocomposites. The reason could be the presence of crystal fraction and orientation in PVC that hinder the establishment of a network for thermal conductivity.[13–16] Furthermore, with the increase of temperature PVC polymeric chains

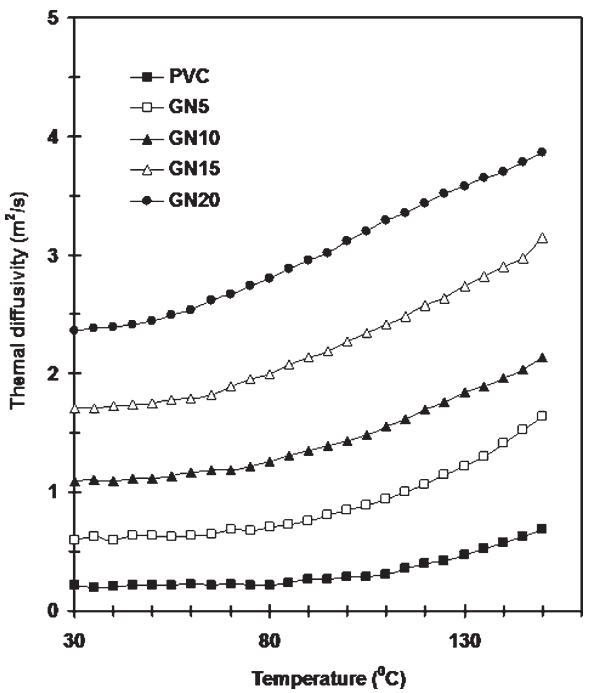

Figure 6 Thermal diffusivity versus temperature of PVC/GN nanocomposites.

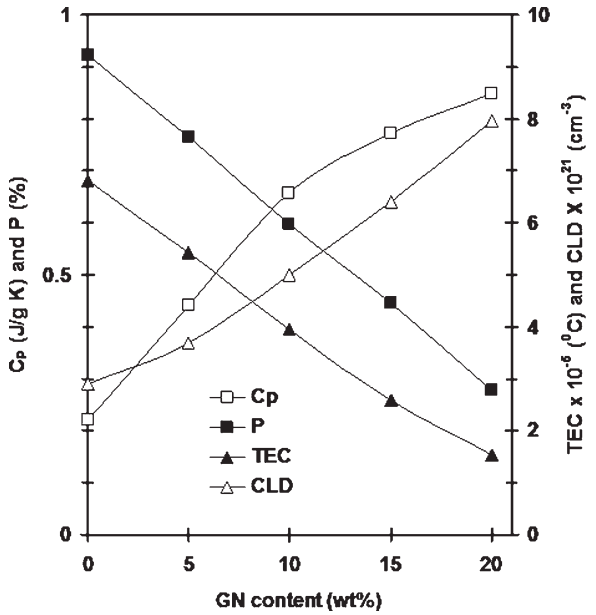

Figure 7 Specific heat (C_p), porosity (p), thermal expansion coefficient (TEC), and cross linking density (CLD).

straighten out more and more and the mean free path of phonons increases resulting in an increase in both the thermal conductivity and diffusivity.[1,2]

Mechanical properties

To gain more deep insight on the above facts, we measured the mechanical properties of composites such as hardness (H), tensile strength (TS), tensile modulus (TM), and elongation at break (EB) as a function of GN content of PVC/GN composites as shown in Figure 8. Interaction between the GN nanoparticles having large aspect ratio and the PVC chains facilitates stress transfer to the reinforcement phase, resulting in improved tensile properties. It is clear that the tensile strength as well as tensile modulus increase with GN content increase in composites. The increase in the tensile strength and modulus with increase in GN content is due to increase in polymer–filler and filler–filler interactions in PVC/GN composites, which restrict the mobility of PVC chain.[33,35] In addition, the formation of strong interfacial adhesion and good dispersion between filler and matrix could also increase the values of tensile modulus. Also, the increase in tensile strength may be attributed to the fact that high stresses enhance the flow mechanism by increasing the mobility of the macromolecular chains to yield higher flexibility. In Figure 8, the decrease of the elongation at break with increasing GN content is due to decrease of the molecular mobility of composites. This suggests that the GN nanosheets, i.e., plate-like layers, can perform the role of reinforcement in PVC/G composite for the purpose of stiffening the PVC matrix. The stiffness of the GN nanoparticles contributed to the immobilization of PVC segment. The decrease in the elongation at break with increasing GN loadings may be attributed to the formation of graphite tactoids, which effectively weaken the number of available reinforcing links. It was noticed from Figure 8, that the hardness increases significantly from 53 to 91 shore D with increase in the GN content. As hardness depends on the behavior of particulate fillers in the composites, the filler that has strong filler–filler interaction will induce more rigidity. This result clearly indicates that there is enhancement in dimensional stability of these composites with increase in GN content.

Dielectric properties of GN reinforced nanocomposites

The variation of real and imaginary part of permittivity with frequency at room temperature for green PVC and PVC/GN nanocomposites is depicted in Figures 9 and 10, respectively. It is clear that both the real and imaginary part of permittivity increased as the GN content increased into composites. When GN reinforced PVC with different volume content, the real and imaginary permittivity increase due to interfacial polarization.[22,23] This facts can be explained as the follows, in heterogeneous systems where a dielectric material is composed of two or more phases, space charge build up occurs at the macroscopic interface and the accumulation of polar charges at the interface leads to dipolar polarization

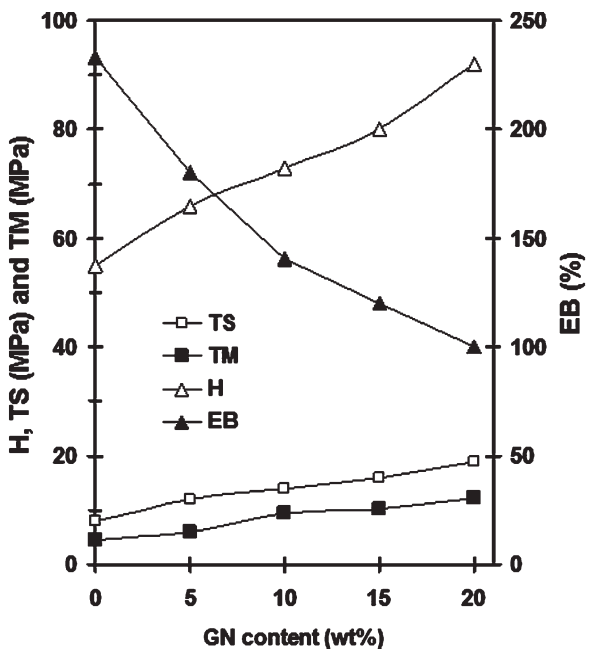

Figure 8 Hardness shore (D), elongation at break (EB), tensile strength (TS), and tensile modulus (TM) of PVC/GN nanocomposites.

as a result of the differences in the dielectric constants of the materials at the interface. This accumulation of space charge leads to field distortions and dielectric loss; this interfacial loss depends on the quantity of filler present as well as on the geometrical shape of its dispersion. The magnitude of the interfacial loss is particularly susceptible to the length of the dispersed phase geometry in the direction of the field. In conclusion, The higher the polarizability of the material greater will be the real and imaginary permittivity.

In Figure 9 it is observed that the real permittivity rapidly decreases with increasing frequency and then slightly decreases. A rapid decrease in real permittivity may be noticed over the frequency range of 1–9 GHz. This can be explained as follows at low frequency the tendency of dipoles in macromolecules to orient themselves in the direction of the applied field and all three types (electronic, atomic, and orientation) of polarizations are taking place.[33,34] The decrease of real permittivity with increase in frequency is due to the orientation of the polarization in the high frequency field. In the case of orientation polarization, the applied field causes a net orientation of the dipoles parallel to the field. On the other hand, in the high-frequency range the dipoles will hardly be able to orient themselves in the direction of the applied field and hence the value of the real permittivity decreases. As the frequency of the applied field is increased, the net polarization is reduced due to orientation polarization and total polarizability falls. This fall in polarizability leads to dielectric relaxation,

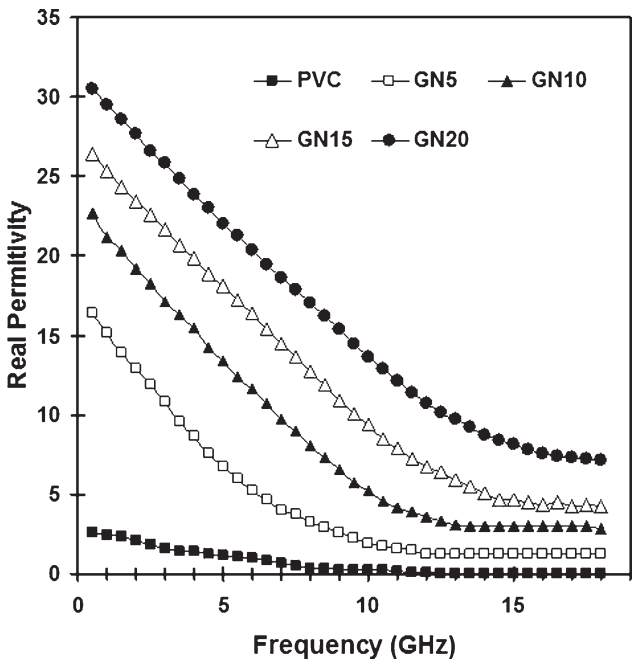

Figure 9 Real permittivity versus frequency for green PVC and PVC/GN nanocomposites.

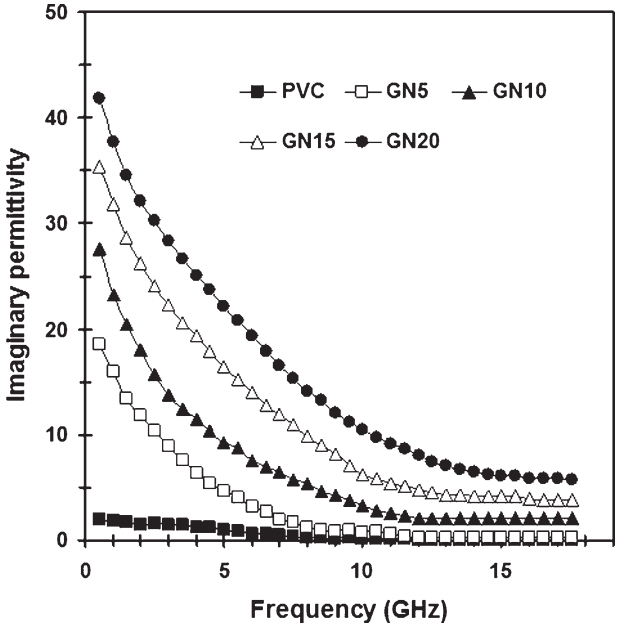

Figure 10 Imaginary permittivity versus frequency for green PVC and PVC/GN nanocomposites.

which in turn, leads to a decrease in real permittivity. In other words at higher frequencies due to the rotational displacement of polar groups under the influence of the electric field, frictional loss increases and it reduces real permittivity.[35]

In Figure 10, the decreases of imaginary permittivity with increasing frequency is ascribed to as frequency increases the dielectric loss factor increases. The dielectric loss is a direct function of the relaxation process, which is due to the local motion of the polar groups. At high frequencies the friction between the molecular chains increases, which leads to a higher dielectric loss. This dielectric loss factor leads to the so called ''conductivity relaxation'. At the relaxation region, the polarization acquires a component out of phase with the field and a displacement current in phase with the field, resulting in thermal dissipation of energy.[36]

CONCLUSION

Nanocomposites based on GN reinforced PVC polymer matrix have been fabricated and their network structure, thermal stability, dielectric properties, and mechanical properties as a function of GN content. This numerical and experimental investigation on thermal conductivity of GN reinforced PVC composites has led to the following specific conclusions:

1. The SEM and XRD analysis showed that the GN nanoparticles were incorporated in the PVC matrix. Furthermore, The GN nanoparticles are in good dispersion and bonding with PVC polymer matrix.

2. Considerable enhancement of thermal stability and mechanical properties in PVC/GN nanocomposites, which is attributed to the well-dispersed and interface adhesion of GN nanoparticles with PVC matrix.
3. The PVC/GN nanocomposite thermal conductivity increases almost nonlinearly with increase of GN content. Moreover, the experimental thermal conductivity of composites agree well with theoretical predictions by Agari model.
4. The real and imaginary permittivity increases with increasing GN content into composites. Both the real and imaginary permittivity decreases with increasing frequency into composites.

The present paper is a result of an international collaboration program between University of Tabuk, Tabuk, Kingdom of Saudi Arabia and the University of Chemical Technology and Metallurgy, Sofia, Bulgaria. The authors gratefully acknowledge the financial support from the University of Tabuk.

References

1. Moon, K. S.; Choi, H. D.; Lee, A. K.; Cho, K. Y.; Yoon, H. G.; Suh, K. S. J Appl Polym Sci 2000, 77, 1294.
2. Bindu, G.; Lonappan, A.; Thomas, V.; Aanandan, C. K.; Mathew, K. T. J Mater Sci 2006, 41, 7419.
3. Fan, Z.; Zheng, C.; Wei, T.; Zhang, Y.; Luo, G. Polym Eng Sci 2009, 112, 2041.
4. Kim, S.; Do, I.; Drzal, L. T. Polym Compos 2009, 3, 1.
5. Takimoto, T.; Onishi, T.; Saito, K.; Takahashi, M.; Uebayashi, S.; Ito, K. Electron Commun Jpn 2007, 90, 48.
6. Kalaitzidou, K.; Fukushima, H.; Drzal, L. T. Compos Sci Technol 2007, 67, 2045.
7. Gabriel, S.; Lau, R. W.; Gabriel, C. Phys Med Biol 1996, 41, 2271.
8. Augustine, R.; Kalappura, U. G.; Laheurte, J. M.; Mathew, K. T. Microwave Opt Lett 2009, 51, 2923.
9. Tu, H.; Ye, L. Polym Adv Technol 2009, 20, 21.
10. Mo, Z.; Shi, H.; Chen, H.; Niu, G.; Zhao, Z.; Wu, Y. J Appl Polym Sci 2009, 112, 573.
11. Droval, G.; Feller, J. F.; Salagnac, P.; Glouannec, P. Polym Adv Technol 2006, 17, 732.
12. Saleem, A.; Frormann, L.; Iqbal, A. Polym Compos 2007, 28, 785.
13. Yasmin, A.; Daniel, I. M. Polymer 2004, 45, 8211.
14. Quan, H.; Zhang, B.; Zhao, Q.; Yuen, R. K. K.; Li, R. K. Y. Compos: Part A 2009, 40, 1506.
15. Ito, K.; Furuya, K.; Okano, Y.; Hamada, L. Electron Commun Jpn 2001, 84, 67.
16. Kimberly, Y. D.; Barbara, D. T.; Yangsheng, L.; Hasselman, D. P. H. J Am Ceram Soc 1998, 81, 1583.
17. Lonappan, A.; Hamsakkutty, V.; Bindu, G.; Jacob, J.; Thomas, V.; Mathew, K. T. Microwave Opt Technol Lett 2004, 42, 500.
18. Yohannan, J.; Jacob, J.; Lonappan, A.; Mathew, K. T. Microwave Opt Technol Lett 2003, 39, 112.
19. Zunli, M.; Yinxia, S.; Hong, C.; Ping, Z.; Dandan, Z.; Yanzhi, L.; Hejun, L. Polymer 2005, 46, 12670.
20. Subodh, G.; Deepu, V.; Mohanan, P.; Sebastian, M. T. J Phys D: Appl Phys 2009, 42, 225501.
21. Subodh, G.; Deepu, V.; Mohanan, P.; Sebastian, M. T. Polym Eng Sci 2009, 49, 1218.
22. Jayasundere, N.; Smith, V. J Appl Phys 1993, 73, 2462.
23. Xie, S.-H.; Zhu, B.-K.; Wei, X.-Z.; Xu, Z.-K.; Xu, Y. Compos: Part A 2005, 36, 1152.
24. Kumlutas, D.; Tavmana, I. H.; Coban, M. T. Compos Sci Technol 2003, 63, 113.
25. Ruiying, L.; Tao, L.; Jinsong, L.; Hongbo, Z.; Zhijun, C.; Guanglai, T. Ceram Int 2005, 31, 911.
26. Volkan, C.; Ismail, H. T.; Mediha, K.; Yildirim, A. Polym Compos 2009, 1299.
27. Rebecca, A. H.; Julia, A. K.; Rachel, M. P.; Jason, M. K. J Appl Polym Sci 2008, 109, 2145.
28. Anjana, P. S.; Deepu, V.; Uma, S.; Mohanan, P.; Philip, J.; Sebastian, M. T. J Polym Sci Part B: Polym Phys 2010, 48, 998.
29. Haoming, T.; Lin, Y. Polym Adv Technol 2009, 20, 21.
30. Xiaowen, Z.; Lin, Y. J Appl Polym Sci 2009, 111, 759
31. Wang, Q. I.; Jun, G.; Ru, W.; Zhengkun, H. Polym Compos 2001, 22, 97.
32. Erik, H. W.; Matthew, L. C.; Julia, A. K. J Appl Polym Sci 2003, 88, 112.
33. Rebecca, A. H.; Julia, A. K.; Rachel, M. P.; Jason, M. K. J Appl Polym Sci 2008, 109, 2145.
34. Wenying, Z.; Caifeng, W.; Tao, A.; Ke, W.; Fenjuan, Z.; Hongzhi, G. Compos: Part A 2009, 40, 830.
35. Goyal, R. K.; Samant, S. D.; Thakar, A. K.; Kadam, A. J Phys D: Appl Phys 2010, 43, 1.
36. Kader, M. A.; Kim, K.; Lee, Y.-S.; Nah, C. J Mater Sci 2006, 41, 7341.
37. Al-Ghamdi, A. A.; El-Tantawy, F.; Abdel Aal, N.; El-Mossalamy, E. H.; Mahmoud, W. E. Polym Degrad Stab 2009, 94, 980.
38. El-Tantawy, F.; Abdel-Kader, K. M.; Kaneko, F.; Sung, Y. K. Eur Polym J 2004, 40, 415.
39. Al-Hartomy, O. A.; Al-Solamy, F.; Al-Ghamdi, A. A.; Ibrahim, M. A.; Dishovsky, N.; El-Tantawy, F. J Elast Plast 2011, 43, 137.